Published in final edited form as:
J Mol Biol. 2009 February 27; 386(3): 717–732. doi:10.1016/j.jmb.2008.12.063.

Investigation of the Biophysical and Cell Biological Properties of Ferroportin, a Multi-Pass Integral Membrane Protein Iron Exporter

Adrian E. Rice[1], **Michael J. Mendez**[2,3], **Craig A. Hokanson**[2], **Douglas C. Rees**[3,4], and **Pamela J. Björkman**[2,4]

1 *Graduate Option in Biochemistry and Molecular Biophysics, California Institute of Technology, Pasadena, California 91125*

2 *Division of Biology, California Institute of Technology, Pasadena, California 91125*

3 *Division of Chemistry and Chemical Engineering, California Institute of Technology, Pasadena, California 91125*

4 *Howard Hughes Medical Institute, California Institute of Technology, Pasadena, California 91125*

Abstract

Ferroportin is a multi-pass membrane protein that serves as an iron exporter in many vertebrate cell types. Ferroportin-mediated iron export is controlled by the hormone hepcidin, which binds ferroportin, causing its internalization and degradation. Mutations in ferroportin cause a form of the iron overload disease hereditary hemochromatosis. Relatively little is known about ferroportin's properties or the mechanism by which mutations cause disease. Here we expressed and purified human ferroportin to characterize its biochemical/biophysical properties in solution and conducted cell biological studies in mammalian cells. We show that purified, detergent-solubilized ferroportin was a well-folded monomer that bound hepcidin. In cell membranes, the N- and C-termini were both cytosolic, implying an even number of transmembrane regions, and ferroportin was mainly localized to the plasma membrane. Hepcidin addition resulted in a redistribution of ferroportin to intracellular compartments that labeled with early endosomal and lysosomal, but not Golgi, markers and that trafficked along microtubules. An analysis of 16 disease-related ferroportin mutants revealed that all formed well-folded monomers that localized to the plasma membrane, but some were resistant to hepcidin-induced internalization. The characterizations reported here form a basis upon which models for ferroportin's role in regulating iron homeostasis in health and disease can be interpreted.

Introduction

Hereditary hemochromatosis is an iron overload disease caused by defects in the regulation of cellular and systemic iron levels.[1,2] One type of hemochromatosis, type IV hereditary hemochromatosis or ferroportin disease, is caused by missense mutations in the gene encoding the iron export protein ferroportin (Fpn, also known as IREG1 or MTP1; accession #**Q9NP59**).[3] Fpn is a multi-pass integral membrane protein found in vertebrates.[4–6] All cell types that export ionic iron express Fpn, including duodenal enterocytes, white blood cells involved in erythrophagocytosis, Kupffer cells, brain astrocytes and placental cells.[4–7]

Address correspondence to: Pamela J. Björkman, Ph.D., 1200 E California Blvd, MC 114-96, Pasadena CA, 91125. Fax: (626) 792-3683; E-mail: E-mail: bjorkman@caltech.edu.

Although Fpn has been implicated as the iron exporter in these cells, whether this export process is active or passive is unknown. Fpn expression levels are regulated post-translationally by interaction with hepcidin-25, a peptide hormone[8] produced in the liver[9] and secreted into the blood when iron levels are high.[10] Hepcidin binds to Fpn at the cell surface and is internalized with Fpn.[8] In HEK293T cells, and presumably *in vivo*, the binding of hepcidin to Fpn results in the phosphorylation, ubiquitination and internalization of Fpn,[11] ultimately leading to its degradation in lysosomes.[8]

Ferroportin disease usually presents as one of two phenotypes – one in which patients display macrophage iron loading, low transferrin iron saturation, and high serum ferritin levels; and one in which patients display hepatocyte iron loading and high transferrin saturation. A number of point mutations in the Fpn gene have been identified.[3,12–25] Recent *in vitro* studies have focused on characterizing subsets of these mutants in an effort to reveal the nature of the defects caused by the disease-causing Fpn mutations.[26–31]

Here we report recombinant expression of Fpn in insect cells, and a biophysical characterization of purified, detergent-solubilized Fpn, including a determination of its oligomeric state and its binding interactions with different forms of hepcidin. We also compared the expression and sub-cellular localization of wild-type and mutant Fpn in the presence and absence of hepcidin and study wild-type Fpn-trafficking using live-cell imaging.

Results

Expression and characterization of Fpn expressed in insect cells

Human, mouse and zebrafish Fpn was expressed in baculovirus-infected insect cells. Expression constructs were created encoding tagged versions of full length human, mouse and zebrafish Fpns. Addition of an N-terminal Rho tag, the first 20 amino acids of bovine rhodopsin, which boosts expression levels for some eukaryotic membrane proteins,[32] was required for detectable expression in insect cells. C-terminal FLAG and/or His tags were added to aid in affinity purification, resulting in Rho-Fpn-His-FLAG and Rho-Fpn-His constructs. Insect cell membranes were analyzed by fractionation analysis using a discontinuous sucrose gradient,[33] and Fpn was found in the plasma membranes of infected cells (data not shown). Several different detergents could be used to solubilize Fpn from isolated plasma membranes, including [3-[(3-cholamidopropyl)-dimethylammonio]-1-propane sulfonate (CHAPS), 6-cyclohexyl-1-hexyl-β-D-maltoside (CYMAL-6), lauryldimethylamine-N-oxide (LDAO) and polyoxyethylene(8)dodecyl ether ($C_{12}E_8$), n-decyl-β-D-maltoside (DM), and n-dodecyl-β-D-maltoside (DDM). Human Rho-Fpn-His and Rho-Fpn-His-FLAG were purified in DM or DDM using affinity chromatography with yields of ~ 50–100 μg Fpn per liter of insect cell culture. Similar results were obtained for mouse and zebrafish Fpns, but the analyses reported in the remainder of this study were conducted using human Fpn. More highly purified Fpn was obtained from the Rho-Fpn-His-FLAG construct using a two-step His/FLAG affinity purification protocol. SDS-PAGE analysis of purified Rho-Fpn-His and Rho-Fpn-His-FLAG revealed a single predominant band migrating with an apparent molecular mass of ~ 60 kDa (Figure 1A). Western analysis showed this band to be positive for both the N-and C-terminal tags, thus demonstrating expression of full-length Fpn (data not shown).

To verify biological activity, we evaluated the ability of purified, detergent-solubilized human Fpn to bind hepcidin. Rho-Fpn-His was purified from insect cell membranes in DM or DDM on a cobalt affinity resin, and then captured on a CM5 biosensor surface with an immobilized anti-Rho antibody. Hepcidin-25 or a non-Fpn-binding version lacking the five N-terminal amino acids (hepcidin-20)[8] was injected at 10 μM. In three independent experiments, we found that ~ 10-fold more hepcidin-25 than hepcidin-20 bound to the Fpn surface (Figure 1B). In an attempt to obtain an equilibrium dissociation constant (K_D) for the interaction between Fpn

and hepcidin-25, surface plasmon resonance binding experiments between coupled Fpn and a dilution series of hepcidin-25 (0.625 – 10 μM) were performed (Figure 1B). While the data did not fit well to a 1:1 binding model, presumably due to complex binding events related to aggregation of the injected hepcidin (see Methods), the results suggested a low micromolar K_D.

Detergent-solubilized Fpn is monomeric

In order to determine the molecular mass, and hence the oligomeric state, of purified Fpn, size exclusion chromatography (SEC) was performed in conjunction with multi-angle light scattering (LS), differential refractive index (RI), and ultraviolet absorption spectroscopy analysis (UV).[34] SEC-LS/UV/RI can be used determine the absolute molecular mass of a protein in complex with non-UV-absorbing modifiers, such as carbohydrates, lipids or detergents.[34,35] Purified human Fpn (Rho-Fpn-His-FLAG) solubilized in DDM was used for these experiments. The UV chromatogram for Fpn was observed as a single peak at ~ 13.5 mL, whereas the LS and RI traces were both doublets, with one peak at ~ 13.5 mL and another at ~ 15.5 mL (Figure 1C). The first peak in the doublets overlaid with the UV peak and corresponded to the Fpn-detergent micelle complex, while the second peak corresponded to free detergent micelles. The free-micelle peak of DDM detergent gave a calculated molecular mass of 75.8 ± 6.8 kDa, consistent with the DDM micelle size measured by the vendor (http://www.anatrace.com). Although the Fpn-detergent peak was not fully resolved from the DDM free micelle peak, large regions of each peak were sufficiently separated and could be selected for analysis (Figure 1C). The molecular mass of the Fpn-detergent complex determined using this method was 201 ± 18 kDa, with 69.1 ± 6.2 kDa of this attributed to protein and 132 ± 12 kDa attributed to bound detergent plus lipids and/or carbohydrate. The molecular mass derived for the protein component of the Fpn-detergent complex is in agreement with the predicted molecular mass of 69,015 g/mol for Rho-Fpn-His-FLAG, thus suggesting that detergent-solubilized Fpn is a monomer.

Topology of Fpn in the plasma membrane

The location of the N- and C-termini of Fpn has been the subject of debate, with some studies finding one or both termini to be extracellular[27,28,36] and others finding one or both termini to be intracellular.[26,37,38] In order to resolve this issue, we expressed N- and C-terminally tagged Fpn (Rho-Fpn-GFP) in three different mammalian cell lines and used confocal immunofluorescence microscopy to compare the accessibility of the tags in permeabilized versus non-permeabilized cells. Although the Rho tag was required for expression in insect cells, we found that Fpn could be expressed in mammalian cells without this tag, so we evaluated the location of the C-terminus in independent experiments. If the N- or C-terminus were extracellular, we would expect to find no difference in permeabilized versus non-permeabilized cells when probing with an antibody against the relevant tag. If a terminus was intracellular, we would expect to see antibody staining in permeabilized, but not unpermeabilized, cells.

Fpn-GFP or Rho-Fpn-GFP constructs were transiently expressed in HEK293T, HeLa and Madin-Darby Canine Kidney (MDCK) cells. Both constructs were used to determine the location of the C-terminus using a labeled anti-GFP antibody, and the Rho-Fpn-GFP construct was used to determine the location of the N-terminus using a labeled anti-Rho antibody. Full confocal stacks were recorded for each condition with representative slices displayed in Figures 2 and 9. GFP-fluorescence from the C-terminal tag was visible at the plasma membrane under permeabilizing and non-permeabilizing conditions, and served as a marker for successfully transfected cells. Antibody staining of the N-terminal Rho or the C-terminal GFP tag was only observed under permeabilizing conditions or when the plasma membrane was compromised by a visible tear. This result was consistent for both Rho-Fpn-GFP and Fpn-GFP in three cell

lines (Figure 2 and 9). We conclude that both the N- and C-termini of Fpn are cytosolic in HeLa, HEK293T, and MDCK cells, implying that Fpn contains an even number of transmembrane domains.

Disease-related Fpn mutants behave like wild-type in detergent and are expressed at the plasma membrane

To determine if disease-related mutations in Fpn altered its detergent-solubility and oligomeric state, we expressed 16 different Fpn-GFP mutants transiently in HEK293T cells and compared them to wild-type Fpn-GFP. Rather than purify each of the mutants and conduct SEC-LS/UV/RI experiments, we used fluorescent size exclusion chromatography (FSEC), a method to obtain an SEC profile of a GFP-tagged protein in a complex mixture of proteins.[39] We found that the FSEC traces for Fpn-GFP and the suite of disease-causing mutant proteins were similar (Figure 1D). Given that SEC-LS/UV/RI analysis demonstrated that wild-type Fpn is well-folded (i.e., it migrates in SEC as a defined peak outside of the void volume) and a monomer (Figure 1C), the finding of similar SEC profiles for wild-type and mutant Fpns indicates that the mutants were also well-folded monomers that could be solubilized in detergent.

We next determined the subcellular localizations of wild-type and mutant Fpn-GFP proteins expressed transiently in different cell lines. Expression of wild-type Fpn-GFP in polarized cells (filter-grown MDCK cells) revealed that Fpn-GFP was expressed primarily on the cell surface (Figure 3). Expression was observed along the entire basolateral membrane below the tight junctions, but not at the apical surface, as determined by anti-ZO1 staining of the tight junctions (data not shown). In an unpolarized cell line (HeLa), fluorescence for wild-type Fpn-GFP was found around the entire cell surface as well as in intracellular compartments (Figure 2), as previously described for expression in HeLa and HEK293T cells.[8] Upon treatment with the protein synthesis inhibitor cycloheximide, a larger proportion of Fpn-GFP localized to the plasma membrane and the intracellular Fpn-GFP signal that remained was faint and diffuse compared to the fluorescence at the plasma membrane (Figure 4), suggesting that much of the intracellular Fpn-GFP signal observed in untreated cells represented newly synthesized protein on its way to the cell surface.

The localization of each of the disease-related Fpn mutants was examined in cycloheximide-treated HeLa cells (Figure 4) and in untreated filter-grown polarized MDCK cells (Figure 3). Each of the mutants localized similarly to wild-type Fpn-GFP; i.e., with little internal fluorescence and a strong cell surface signal. Evidence for the primarily surface localization of Fpn-GFP proteins can be difficult to convey in 2D images of flat HeLa cells, so we present side views of cells for all the Fpn mutants (Figure 4) and movies of 3D reconstructions for selected mutants (Movies S1-S5). These data suggested that all of the disease-related Fpn mutants examined here trafficked normally to the plasma membrane.

Effects of hepcidin on disease-related Fpn mutants

Previous studies demonstrated that wild-type Fpn is internalized into lysosomes upon treatment with hepcidin-25.[8] To compare the effects of hepcidin on wild-type and mutant Fpns, we expressed Fpn-GFP proteins transiently in HeLa cells, pretreated the cells with cycloheximide to reduce intracellular fluorescence, and then incubated in the presence or absence of 2 μM hepcidin-25. After 4 hours, the cells were fixed and examined by confocal fluorescence imaging. Wild-type Fpn-GFP was internalized in all cells imaged, but the level of internalization at any tested time point varied from cell to cell. At the 4 hour time point used for this study, the GFP signal in some cells was observed as fully internalized puncta, whereas other cells displayed a portion of their GFP signal at the plasma membrane (see the two wild-type Fpn-GFP panels in Figure 4). The surface signal tended to decrease over time as the

hepcidin-25 incubation progressed (data not shown). We expect these differences were due to varying levels of Fpn-GFP expression from cell to cell in the transient transfection.

Most of the disease-related Fpn mutants were internalized upon treatment with hepcidin-25 (Figure 4), with internalization observed as bright puncta throughout the cytoplasm. Hepcidin-sensitive Fpn-GFP constructs included wild-type Fpn, and the A77D, N144D, N144H, N144T, D157G, ΔV160, N174I, Q182H, Q248H, D270V, and G323V Fpn mutants. Like wild-type Fpn-GFP, the hepcidin-sensitive Fpn-GFP mutants displayed a distribution of internalization completeness, with some cells within a sample showing residual surface signals. Representative cells from these experiments can be found in Figure 4. The Y64N, G80S, C326S, C326Y, and G490D Fpn mutants showed no internalized puncta and therefore classified as resistant to hepcidin-induced internalization (Figure 4).

Characterization of hepcidin-induced Fpn internalization in HeLa cells

To further study the pathway by which Fpn is internalized upon treatment with hepcidin, we identified Fpn-positive compartments using antibodies against endosomal and lysosomal markers. For these experiments, wild-type Fpn-GFP was transiently expressed in HeLa cells, pre-treated with cycloheximide, and then incubated with hepcidin-25 for 4 hours, as described above. Cells were fixed and probed with fluorescent antibodies against the early endosomal marker EEA1, the lysosomal markers LAMP1 or LAMP2, or a 58 kDa Golgi-resident protein. Internalized Fpn-GFP puncta were found to partially co-localize with EEA1, LAMP1 and LAMP2, but not with the 58 kDa Golgi marker (Figure 5).

Hepcidin-induced internalization of Fpn-GFP was also investigated in live HeLa cells using spinning-disk confocal microscopy, which enables rapid image acquisition to monitor dynamic biological processes.[40] Fpn-expressing HeLa cells were grown in glass-bottomed dishes and imaging was performed at 37° C in a temperature-controlled enclosure. Fpn-GFP-positive intracellular compartments, which were observed within 15 minutes of hepcidin addition, were seen to travel throughout much of the cytoplasm in a relatively random fashion (data not shown). Over the course of hours, accumulation of bright puncta in regions proximal to the nucleus was observed, as seen in the fixed cell images, which were acquired 4 hours after hepcidin addition (Figure 4).

When trafficking was monitored for a shorter time (0.5–5 minutes), Fpn-GFP compartments traveled in many directions with no apparent net directionality. Interestingly, some of the Fpn-GFP-positive compartments moved back and forth along what appeared to be a track. To determine if the tracks represented microtubules, we imaged the cells in the presence and absence of the microtubule depolymerizing agent nocodazole. In the presence of nocodazole, trafficking of Fpn-GFP positive compartments was almost entirely halted (Figure 6, Movies S6 and S7). Tracking analyses were performed on > 1100 Fpn-positive compartments per condition and the disruption of overall trafficking by nocodazole was evident in terms of a reduction of mean squared displacement for individual compartments (Figure 7A) and in a reduction of overall track displacement length for the full set of tracks (Figure 7B). In the presence of nocodazole, no compartments were found more than 0.98 μm from their starting points, whereas in untreated cells, 178 compartments (15.9%) were located at a distance of 1 μm or further from their starting points.

Discussion

Although Fpn plays a key role in the maintenance and regulation of systemic iron homeostasis, many of its basic features remain controversial. We sought to characterize some of the biophysical and cell biological properties of Fpn using purified, detergent-solubilized protein

and Fpn expressed in eukaryotic cells. Here we report an insect cell expression system that can be used to produce recombinant human Fpn for structural and biophysical studies.

The oligomeric state of Fpn has been debated for several years – the protein has been reported to be a monomer[36,38,41] or a dimer/multimer.[30,37] Using SEC-LS/UV/RI, a shape- and model-independent method to obtain a molecular mass,[34] we determined that purified detergent-solubilized Fpn is monomeric (Figure 1C). This result does not explicitly address the oligomeric state of Fpn in its native environment of the lipid bilayer. However, in previous studies of other membrane proteins, including LacY and GlyT1, the oligomeric state determined for the purified protein in detergent correlated with the oligomeric state in the membrane bilayer.[42,43] Thus although this result cannot rule out a transient dimerization/multimerization event, it suggests that homophilic interactions that might exist in the context of a bilayer are sufficiently weak so as to be disrupted by a non-ionic detergent. A recent report has shown that a 19-amino acid peptide derived from an extracellular loop of Fpn (the hepcidin-binding domain; residues 324 to 343) is capable of binding hepcidin-25 but not hepcidin-20.[44] In support of the contention that purified Fpn monomers are functional, we showed that purified Fpn exhibits physiologically-relevant binding to hepcidin-25, but not hepcidin-20 (Figure 1B), suggesting that detergent-solubilized Fpn effectively presents the hepcidin-binding domain. Although we were unable to obtain an accurate K_D for the Fpn/hepcidin-25 interaction, the data suggested a low micromolar affinity, consistent with the ~ 0.7 μM IC_{50} value obtained *in vitro*[8] and *in vivo* experiments in which a serum concentration of 1.4 μM hepcidin-25 induced a prolonged reduction in serum ferritin levels.[45]

The membrane topology of Fpn and the related issue of how many transmembrane domains it contains have also been the subject of debate. In particular, different results have been obtained for the location of the Fpn C-terminus. Fluorescent antibodies against a C-terminal tag on Fpn have been used to label live cells in flow cytometry experiments,[27,28,36] implying an extracellular location. Immunofluorescence microscopy has been used to suggest both an extracellular[36] and an intracellular[26,37,38] localization for the Fpn C-terminus. Our results using two different ferroportin constructs in three different mammalian cell lines strongly support an intracellular location for both the N- and C-termini of Fpn. A recent report may explain the discrepancy in the studies regarding the accessibility of the Fpn termini: the C-terminus of Fpn was found to be normally cytosolic, but accessible to labeled antibodies in non-permeabilized cells when the cells were undergoing apoptosis due to reduced intracellular iron levels.[38] Thus previous reports of the detection of C- and N-terminal tags in non-permeabilized cells may have resulted from inclusion of apoptotic cells in the analyses. Assuming that both the N- and C-termini of Fpn are cytosolic, as suggested by our data and some of the previous studies,[26,37,38] Fpn must have an even number of transmembrane spanning domains. Using the prediction software TMHMM[46] and an alignment of human, mouse, and zebrafish Fpn sequences, we predicted that Fpn contains 12 transmembrane domains (Figure 8), differing from prior predictions of 9 or 10 membrane spanning regions,[4,5,13] but similar to a recent prediction published in conjunction with insertion mutagenesis analyses.[26] Our model places the tyrosines that become phosphorylated upon hepcidin-25 binding, Y302 and Y303,[11] in the middle of transmembrane region 6 (TM6), and thus not accessible to cytosolic kinases. The model may be inaccurate in the region of TM6, or alternatively, the binding of hepcidin-25 to the extracellular loop located between TM6 and TM7 could cause a conformational shift that adjusts the location of TM6 such that Y302 and Y303 become accessible to the cytosol where they can be phosphorylated.

Although Fpn has been reported to be predominantly localized to the plasma membrane in the absence of the peptide hormone hepcidin, previous studies showed visible internal staining when Fpn was stably or transiently expressed in HEK293T cells.[8,27–30,36] Here we showed that most of the internal Fpn-GFP signal was eliminated by treatment with the protein synthesis

inhibitor cycloheximide when Fpn-GFP was transiently expressed in HeLa cells (Figure 4). Having worked out conditions such that the majority of wild-type Fpn was localized to the plasma membrane in the absence of hepcidin, we were able to rapidly screen the localization of disease-related Fpn mutants in the presence and absence of hepcidin.

Upon treatment with cycloheximide in the absence of hepcidin, we found that wild-type Fpn-GFP and 16 of 16 disease-related Fpn-GFP mutants tested in this assay localized primarily to the plasma membrane of HeLa cells (Figure 4). These results conflict with some studies conducted in the absence of cycloheximide; for example, one report suggesting that the A77D Fpn mutant is intracellular[29] and others suggesting that the A77D,[26] D157G,[26] ΔV160,[26,30,36] N174I,[29] G323V,[30,36] and G490D[30] Fpn mutants exhibited partial internalization. The discrepancies may reflect cell-type specific differences in folding rates, thus slowly-folding mutants might appear to be intracellular in cells that were not treated with cycloheximide. This is clearly not the case for all cells, however, as we observed primarily plasma membrane localization for wild-type Fpn-GFP and the 16 disease-related mutants in polarized MDCK cells, in which case the use of cycloheximide to eliminate intracellular signals was not necessary (Figure 3).

Using the cycloheximide treatment procedure for reproducibly expressing Fpn-GFP on the surface of HeLa cells, we next investigated the responses of Fpn mutants to hepcidin treatment. As previously described,[8] we found that wild-type Fpn-GFP was internalized by the addition of hepcidin-25 to HeLa cells (Figure 4). In our experiments, we saw internalization of the Fpn-GFP signal within an hour of incubation with 2.0 μM hepcidin-25, and by four hours of incubation, the Fpn-GFP signal in many cells was entirely intracellular. Our experiments showed that the internalized Fpn-GFP passes through EEA1- and LAMP-positive compartments but does not accumulate in the Golgi (Figure 5), and that this trafficking is dependent on intact microtubules (Figure 6).

There was some variability in the degree of wild-type Fpn-GFP internalization in hepcidin-treated cells, presumably due to different expression levels in the transiently-transfected cells, and thus we did not attempt to quantify relative levels of Fpn internalization for each of the mutants. Instead, we considered a Fpn mutant to be hepcidin-sensitive if we observed distinct internal Fpn-GFP puncta after a 4 hour incubation with 2 μM hepcidin-25 (a concentration chosen to ensure saturation), and hepcidin-resistant if no distinct puncta were observed. Using these definitions, we report that the Fpn-GFP mutants A77D, N144D, N144H, N144T, D157G, ΔV160, N174I, Q182H, Q248H, D270V, and G323V were hepcidin-sensitive, and that the Fpn-GFP mutants Y64N, G80S, C326S, C326Y, and G490D were hepcidin-resistant (Figure 4). The N144T, D270V, and C326S Fpn mutants had not been tested for hepcidin internalization prior to this report. Some of the results for the other mutants conflict with prior studies, whereas others are in agreement. For example, one study reported N144H, D157G, ΔV160 and G323V as hepcidin-resistant, yet agreed with our results that G490D was resistant and that Q182H was sensitive.[30] Another study differed from our results by reporting that the A77D and N174I mutants were hepcidin-resistant and the G80S mutant was hepcidin-sensitive.[29] A third study reported A77D, N144H, D157G, V160, Q182H and G323V all as hepcidin-resistant.[26] These discrepancies may have arisen from different experimental conditions – the analyses described in these studies were performed without cycloheximide pre-treatment and using a lower hepcidin-25 concentration of 0.36 μM or 0.7 μM. However, an additional study, using a cycloheximide pre-treatment and a 0.5 μM hepcidin-25 concentration, agreed with our results that Y64N and C326Y were hepcidin-resistant and that N144D, N144H, and Q248H were at least partially internalized upon hepcidin treatment.[28] It should be noted that our analysis does not distinguish between Fpn mutations within the hepcidin-binding site that cause a reduced affinity for hepcidin, and mutations that prevent the Fpn-hepcidin complex from interacting properly with internalization machinery.

Linking the phenotypic manifestations of iron overload in patients affected by ferroportin disease caused by specific mutations with *in vitro* analyses on those same Fpn mutants has been difficult. This is due to the heterogeneity of patient phenotypes even between family members sharing the same Fpn mutation, the lack of data for patients affected by certain mutations, and the difficulty of working with Fpn *in vitro* (as demonstrated by the conflicting experimental results reported to date). However, by combining our results with available clinical data, the data presented in our study support a model in which Fpn mutations resulting in hepcidin resistance *in vitro* manifest themselves as a disease with high transferrin saturation (observed in Y64N and C326S),[16,25] low to moderately high serum ferritin levels (observed in Y64N and C326S),[16,25] and hepatocyte iron loading (observed in Y64N, C326S and G490D),[16,20,25] whereas Fpn mutations resulting in hepcidin sensitivity *in vitro* would produce disease with low transferrin saturation (observed in A77D, D157G, ΔV160, N174I, Q182H, Q248H and G323V),[13–15,17,21,22,47–49] high serum ferritin (observed in A77D, N144D, N144H, N144T, D157G, ΔV160, N174I, Q182H, Q248H and G323V),[13–15,17–19,21,22,47–50] and mostly macrophage/Kupffer cell iron loading with additional hepatocyte iron loading in extreme cases (observed in A77D, N144D, N144H, N144T, ΔV160 and N174I).[13,14,18,19,47–50]

Materials and methods

Insect cell expression of Fpn

Genes encoding human and mouse Fpns were gifts of Alain Townsend (Oxford) and the zebrafish Fpn gene was the gift of Nancy Andrews (Duke University School of Medicine). Human, mouse, and zebrafish Fpn were expressed in a lytic baculovirus/insect cell expression system. A Rho tag was added to each construct using PCR by replacing the Fpn start codon with the first 20 amino acids of bovine rhodopsin and a linker (nucleic acid sequence: ATGAACGGGACCGAGGGCCCAAACTTCTACGTGCCTTTCTCCAACAAGACGGGC GTGGTAGGCCGGCCGCGGCCGCGA). The C-termini of the insect cell constructs were tagged with 10x-Histidine (Rho-Fpn-His) or tandem 10x-Histidine and FLAG tags (Rho-Fpn-His-FLAG) and a linker (nucleic acid sequence: AGCGGCCGCGAAAACTTGTACTTTCAAGGCCATCACCATCACCATCACCATCAC CATCACGACTACAAGGACGACGACGACAAGGGCGCGCCT). Constructs were subcloned into pBacPAK8 (Clontech) and viruses were constructed using ProGreen Baculovirus DNA (AB Vector). GFP-expression was used to titrate the virus required to attain > 95% infection. For protein expression, 5 L of High Five insect cells in ESF 921 media (Expression Systems) were grown using a 20/50EH Wave Bioreactor (GE Healthcare) (settings: rocking speed 9; angle 20°; temp 27° C, and ambient air pumped in at 0.3 L/min). Cells were infected at a density of 2.5–3.5 × 10^6 viable cells/mL and were harvested 48 hours after infection.

Solubilization of Fpn from membranes

All steps were performed on ice or at 4° C. Cell paste (110–140 g) was resuspended in 900 mL resuspension buffer (50 mM Tris pH 7.5, 150 mM NaCl, and 18 EDTA-free complete protease inhibitor tablets (Roche)). Cells were disrupted by sonication in 50 mL fractions on ice and placed in an ice bath between sonication rounds. Cell debris and membranes were pelleted at 125,000×g.

Membrane pellets were resuspended using a Dounce homogenizer in 300 mL detergent-free solubilization buffer (50 mM Tris pH 7.5, 500 mM NaCl, 10 mM imidazole pH 7.5, and 6 EDTA-free complete protease inhibitor tablets (Roche)). Dry n-decyl-β-D-maltoside (DM; Anatrace) or n-dodecyl-β-D-maltoside (DDM; Anatrace) was added to 1% (w/v) to

resuspended membranes and incubated with gentle stirring at 4° C for 2.5 hours. After pelleting at 125,000×g, membrane suspensions were filtered at 0.45 μm.

Affinity purification of Fpn

Detergent-solubilized Fpn was purified by single (Rho-Fpn-His) or double (Rho-Fpn-His-FLAG) affinity steps. For His tag purifications, TALON-superflow columns (TALON) were pre-equilibrated with solubilization buffer containing 0.02% (w/v) DDM. Supernatants were passed over the column and washed to baseline. Non-specific binders were washed off with equilibration buffer containing 30 mM imidazole, and Fpn was eluted with buffer containing 120 mM imidazole.

Rho-Fpn-His-FLAG was further purified using an anti-FLAG M2 affinity column (Sigma) equilibrated in TALON elution buffer. TALON eluates were passed over the affinity column twice, which was washed with M2 buffer (50 mM Tris pH 7.5, 150 mM NaCl, and 0.02% (w/v) DDM) and eluted with M2 buffer containing 0.2 mg/mL FLAG peptide (Sigma). Boiling of samples in SDS sample buffer resulted in aberrant migration near the top of a SDS-PAGE gel, so gel samples were not boiled prior to loading.

Molecular mass and oligomeric state determination by SEC-LS/UV/RI

Size exclusion chromatography (SEC) was conducted with in-line multi-angle static light scattering to determine the molecular mass of purified Fpn. The FLAG column eluate was concentrated to 0.5 mL using a 50 kDa cutoff Amicon Ultra concentrator (Millipore), and passed over a Superdex 200 10/300 SEC column (GE Healthcare) pre-equilibrated in buffer containing 50 mM Tris HCl pH 7.5, 150 mM NaCl and 0.02% (w/v) DDM at 0.5 mL/min. The SEC column was plumbed in line with a multi-angle static light scattering monitor at 658 nm (DAWN Helios, Wyatt), a differential refractive index monitor (Optilab rEX, Wyatt), and a UV absorbance monitor (AKTA Explorer, GE Heathcare). All calculations of molecular mass were performed using the protein conjugate template in the ASTRA 5.3.2 software package (Wyatt). The specific refractive index increment (dn/dc) values used were 0.185 for protein (Wyatt) and 0.133 for DDM.[51] The predicted molecular mass and extinction coefficient for UV absorbance at 280 nm for Rho-Fpn-His-FLAG were calculated from the amino acid sequence as 69,015 g/mol and 83,319 $M^{-1}cm^{-1}$, respectively.[52] Bovine serum albumin (GE Healthcare) was used as a calibration standard.

Fpn-hepcidin binding

Experiments evaluating the interaction between human Fpn and human hepcidin were performed at 25° C using a Biacore 2000 Instrument (GE Healthcare). Interactions between immobilized Fpn on a sensor chip and hepcidin injected over the sensor surface were monitored in real time as resonance units (RUs). An anti-Rho monoclonal antibody (see below) was immobilized at densities ranging from 1000–3000 RUs to the surface of a CM5 biosensor chip using primary amine chemistry as described in the Biacore manual. Purified Rho-Fpn-His in 50 mM Tris pH 7.5, 150 mM NaCl, 0.2% (w/v) DM was injected over the anti-Rho surface, capturing 1000–1500 RUs of Fpn. Flow cells containing immobilized anti-Rho antibody without captured Rho-Fpn-His were used as reference-subtracted negative controls. The sensor surface was monitored for > 12 hrs in the same buffer until a stable baseline was reached. Hepcidin-25 (Bachem) or hepcidin-20 (gift of Prof. T. Ganz, UCLA), diluted in this buffer, was injected over the Fpn surface at various concentrations. The surface was observed to return to baseline after one hour, so no regeneration condition was required. Experiments directly comparing the binding of hepcidin-20 and hepcidin-25 to immobilized Fpn were performed using 10 μM hepcidin injections. For experiments to derive kinetic constants for the hepcidin-25/Fpn interaction, a dilution series (0.625, 1.25, 2.5, 5.0, 8.0, and 10 μM) of hepcidin-25 was injected, and the dissociation and association phases of all curves were

simultaneously fit to derive kinetic constants using BIAevaluation 4.1 (GE Healthcare). The data did not fit well to a 1:1 binding model, which can result if the injected analyte is not homogeneous (e.g., the analyte contains a population of aggregates).[53] An approximate equilibrium dissociation constant (K_D) was calculated from the ratio of dissociation and association rate constants.

Construction and mutagenesis of mammalian expression constructs

Fpn-GFP and Rho-Fpn-GFP mammalian expression vectors were constructed in the pLox +CMV expression vector, containing the CMV promoter and SV40 polyA tail. PCR inserts containing the Fpn-GFP or Rho-Fpn-GFP were produced by bridging-PCR using the Fpn gene and the GFP gene derived from pCGFP-EU.[39] Fpn-GFP mutants were produced using site-directed mutagenesis. All constructs were verified by sequencing.

Mammalian cell culture and transfections

HEK293T, HeLa and MDCK cells were grown in DMEM containing 4.5 g/L D-glucose, 4 mM L-glutamine, 110 mg/L sodium pyruvate (Gibco) with 1x penicillin/streptomycin (Gibco) and 10% (v/v) fetal bovine serum (Atlanta Biologicals). All transfections were performed using lipofectamine 2000 (Invitrogen) as per the manufacturer's instruction. MDCK cells grown on transwell filters were initially seeded into 6-well plates and transfected at ~75% confluency. Twenty-four hours later, cells were treated with trypsin-EDTA and 5×10^5 cells were transferred to 12 mm polyester transwell permeable supports (Costar) with 0.5 mL growth media above and 1.0 mL growth media below the support. To ensure full polarization and tight junction formation, transfected cells were grown for 4 days post-confluency before imaging.

FSEC analysis

Wild-type and mutant human Fpn-GFP constructs were transiently expressed in HEK293T cells in 6-well format. Cells were collected by pipetting 36–40 hours post-transfection, and then pelleted and resuspended in 500 μL solubilization buffer (50 mM Tris pH 7.5, 150 mM NaCl, 1% (w/v) DDM). Resuspended cells were lysed by sonication and solubilization was performed with gentle agitation for 2.5 hours at 4° C. Unsolubilized material was pelleted at 125,000xg. The supernatant was removed and filtered through a 0.22 μm Ultrafree-MC spin filter (Millipore). Filtered supernatant was loaded onto a Superdex 200 10/300 SEC column (GE Healthcare) and Fpn-GFP fluorescence was monitored using an online RF-10AXL fluorescence detector (488 nm excitation, 507 nm emission, Shimadzu). SEC was performed at 0.5 mL/min in 50 mM Tris pH 7.5, 150 mM NaCl, 0.2% (w/v) DDM.

Hepcidin-induced Fpn internalization

HeLa cells were seeded onto poly-lysine coated glass coverslips at 10^6 cells/well in a 6-well format and Fpn-GFP constructs were transfected at ~ 80% confluency. After 20 hours, cells were incubated in media containing 75 μg/mL cycloheximide (Sigma) for two hours. This media was then exchanged for media containing 2.0 μM hepcidin-25 (Bachem) and 75 μg/mL cycloheximide. Each internalization time-point included a negative control in which cells were treated only with cycloheximide. Internalization was stopped by fixing cells at room temperature (~ 22° C) for 15 minutes with 4% (v/v) paraformaldehyde in PBS containing 1 mM $CaCl_2$, 0.5 mM $MgCl_2$, and 0.25 mM $MgSO_4$. Fixed samples were washed twice and directly mounted on glass slides in Pro-long GOLD anti fade mounted media containing DAPI nuclear stain (Invitrogen), or quenched in PBS containing 75 mM NH_4Cl, 20 mM glycine for 10 minutes prior to blocking and further antibody treatments. After quenching, samples were incubated in blocking solution (PBS containing 8% (v/v) goat serum (Gibco) and 0.025% (w/v) saponin (Sigma)) for 30 minutes at room temperature. Primary antibody incubations were performed in blocking solution overnight at 4° C. After primary incubation, cells were washed

3 times in PBS and then incubated in blocking solution containing secondary antibodies for 1 hour at room temperature, fixed in PBS containing 4% (v/v) paraformaldehyde for 30 minutes, washed twice in PBS, and then mounted on glass slides as described above.

Antibodies

A mouse monoclonal anti-Rho tag antibody (hybridoma B630N) was purified from ascites fluid using a protein G affinity column followed by SEC. Other antibodies were purchased or received as gifts as indicated. Primary antibodies and the dilutions used for cell staining were the monoclonal mouse anti-Rho at 1 μg/mL, Alexa-647-conjugated rabbit polyclonal anti-GFP (Invitrogen, cat.#A31852) at 1:500; AC17 mouse monoclonal anti-LAMP2 from E. Rodriguez-Boulan (Cornell University) at 1:1000; rabbit polyclonal anti-LAMP1 (Abcam cat. #ab24170) at 1:500; rabbit polyclonal anti-EEA1 (Santa Cruz Biotech cat. #SC-33585) at 1:100; and mouse monoclonal anti-Golgi 58k protein (Abcam cat. #ab6284) at 1:100. Secondary antibodies and their dilutions were Alexa-647-conjugated goat anti-mouse IgG (Invitrogen cat. #A21235) at 1:500 and Alexa-647-conjugated F(ab′)2 fragment of goat anti-rabbit IgG (Invitrogen cat. #A21246) at 1:500.

Confocal imaging and image processing

Confocal images were recorded on an UltraVIEW ERS Rapid Confocal Imager (Perkin-Elmer) using 63x (Plan-APOCHROMAT 1.4 Oil DIC, Zeiss) or 100x (αPlan-APOCHROMAT 1.46 Oil DIC, Zeiss) objectives. GFP and Alexa-647 fluorophores were excited at 488 nm or 647 nm, respectively, using a 488/548/647 multiline argon/krypton laser (Melles Griot). All fixed cells that were imaged had intact nuclei, as determined by DAPI staining (data not shown). Confocal images shown from fixed samples are representative images from full 3D confocal stacks sampled at 0.25 μm spacing in z. Stacks of imaged HeLa, HEK293T and MDCK cells were assembled and thresholds set in Imaris 6.0.1 (Bitplane) before single representative slices were exported and assembled into figures using Photoshop CS3 (Adobe).

Live imaging and tracking

HeLa cells were grown and transfected in 35 mm poly-lysine coated glass-bottomed microwell dishes (Matek). Two dishes were seeded at a density of 10^6 cells/dish and transfected at ~ 80% confluency the following day with Fpn-GFP. After 20 hours, the media was exchanged for media containing 75 μg/mL cycloheximide lacking phenol red. After two hours, the media was exchanged for phenol red-free media containing 2 μM hepcidin-25 and 75 μg/mL cycloheximide. After another two hours, dishes were chilled on ice and their media was exchanged for phenol red-free media containing 10 μg/mL nocodazole, 2 μM hepcidin-25 and 75 μg/mL cycloheximide, or the same chilled media lacking nocodazole. Samples were incubated for 30 minutes on ice and then moved to an UltraVIEW ERS Rapid Confocal Imager (Perkin-Elmer) with a temperature-controlled housing (Solent Scientific) where they were warmed to 37° C for imaging. Fluorescent micrographs were collected at 100x (αPlan-APOCHROMAT 1.46 Oil DIC, Zeiss) in a single focal plane 1 μm above the glass support and imaged at 4.5 frames per second for 90 seconds per cell. Three cells from each condition were imaged. Fpn-GFP-containing compartments were tracked using the tracking module in Imaris 6.0.1 (Bitplane). Spots and tracks were automatically selected using the following Imaris parameters: estimated diameter = 0.35 μm; threshold = 8; Brownian motion tracking algorithm; max distance = 0.66 μm; and gap size = 3; with minimal manual removal required. Tracks shorter than 10 frames (2.2 seconds) were filtered out of the data set. The final data set includes 1295 tracks for the untreated sample and 1149 tracks for nocodazole-treated sample.

Transmembrane Topology Prediction

DNA sequences for full length human, mouse and zebrafish Fpns were submitted to the TransMembrane Prediction using the Hidden Markov Model (TMHMM v2.0) prediction server.[46] Each sequence was predicted to contain 12 regions that were 21–23 amino acids long with a significant (>60% probability) of being a transmembrane (TM) region. TMHMM marked 10 of these regions as TMs in human and mouse Fpns, and eight in zebrafish Fpn, which upon alignment summed to a total of 11 TMs. A final region with much of its sequence at or above 60% probability of being a TM was not annotated as a TM in any of the three Fpn sequences, but we included it in our model for a final prediction of 12 TMs (Figure 8). The approximate starting and ending points for the predicted TMs (using the residue numbering for human Fpn) are: 12–34, 58–80, 93–115, 125–147, 175–195, 199–221, 293–315, 335–357, 373–395, 450–472, 492–514, and 519–541.

Supplementary Material

Refer to Web version on PubMed Central for supplementary material.

Acknowledgements

We thank members of the Bjorkman lab for critical reading of the manuscript and the Caltech Protein Expression Center for virus construction and high titer virus production. This work was supported by the National Institutes of Health (1R01 DK60770-01 to P.J.B.) and a National Science Foundation Graduate Research Fellowship (A.E.R.).

References

1. Pietrangelo A. Hemochromatosis: an endocrine liver disease. Hepatology 2007;46:1291–301. [PubMed: 17886335]
2. Andrews NC, Schmidt PJ. Iron homeostasis. Annu Rev Physiol 2007;69:69–85. [PubMed: 17014365]
3. Montosi G, Donovan A, Totaro A, Garuti C, Pignatti E, Cassanelli S, Trenor CC, Gasparini P, Andrews NC, Pietrangelo A. Autosomal-dominant hemochromatosis is associated with a mutation in the ferroportin (SLC11A3) gene. J Clin Invest 2001;108:619–23. [PubMed: 11518736]
4. McKie AT, Marciani P, Rolfs A, Brennan K, Wehr K, Barrow D, Miret S, Bomford A, Peters TJ, Farzaneh F, Hediger MA, Hentze MW, Simpson RJ. A Novel Duodenal Iron-Regulated Transporter, IREG1, Implicated in the Basolateral Transfer of Iron to the Circulation. Molecular Cell 2000;5:299–309. [PubMed: 10882071]
5. Donovan A, Brownlie A, Zhou Y, Shepard J, Pratt SJ, Moynihan J, Paw BH, Drejer A, Barut B, Zapata A, Law TC, Brugnara C, Kingsley PD, Palis J, Fleming MD, Andrews NC, Zon LI. Positional cloning of zebrafish ferroportin1 identifies a conserved vertebrate iron exporter. Nature 2000;403:776–781. [PubMed: 10693807]
6. Abboud S, Haile DJ. A novel mammalian iron-regulated protein involved in intracellular iron metabolism. J Biol Chem 2000;275:19906–19912. [PubMed: 10747949]
7. Jeong SY, David S. Glycosylphosphatidylinositol-anchored ceruloplasmin is required for iron efflux from cells in the central nervous system. J Biol Chem 2003;278:27144–8. [PubMed: 12743117]
8. Nemeth E, Tuttle MS, Powelson J, Vaughn MB, Donovan A, Ward DM, Ganz T, Kaplan J. Hepcidin regulates cellular iron efflux by binding to ferroportin and inducing its internalization. Science 2004;306:2090–2093. [PubMed: 15514116]
9. Park CH, Valore EV, Waring AJ, Ganz T. Hepcidin, a urinary antimicrobial peptide synthesized in the liver. J Biol Chem 2001;276:7806–10. [PubMed: 11113131]
10. Pigeon C, Ilyin G, Courselaud B, Leroyer P, Turlin B, Brissot P, Loreal O. A new mouse liver-specific gene, encoding a protein homologous to human antimicrobial peptide hepcidin, is overexpressed during iron overload. J Biol Chem 2001;276:7811–9. [PubMed: 11113132]
11. De Domenico I, Ward DM, Langelier C, Vaughn MB, Nemeth E, Sundquist WI, Ganz T, Musci G, Kaplan J. The molecular mechanism of hepcidin-mediated ferroportin down-regulation. Mol Biol Cell 2007;18:2569–78. [PubMed: 17475779]

12. Njajou OT, Vaessen N, Joosse M, Berghuis B, van Dongen JWF, Breuning MH, Snijders P, Rutten WPF, Sandkuijl LA, Oostra BA, van Duijn CM, Heutink P. A mutation in SLC11A3 is associated with autosomal dominant hemochromatosis. Nature Genetics 2001;28:213–214. [PubMed: 11431687]

13. Devalia V, Carter K, Walker AP, Perkins SJ, Worwood M, May A, Dooley JS. Autosomal dominant reticuloendothelial iron overload associated with a 3-base pair deletion in the ferroportin 1 gene (SLC11A3). Blood 2002;100:695–7. [PubMed: 12091367]

14. Wallace DF, Pedersen P, Dixon JL, Stephenson P, Searle JW, Powell LW, Subramaniam VN. Novel mutation in ferroportin1 is associated with autosomal dominant hemochromatosis. Blood 2002;100:692–4. [PubMed: 12091366]

15. Cazzola M, Cremonesi L, Papaioannou M, Soriani N, Kioumi A, Charalambidou A, Paroni R, Romtsou K, Levi S, Ferrari M, Arosio P, Christakis J. Genetic hyperferritinaemia and reticuloendothelial iron overload associated with a three base pair deletion in the coding region of the ferroportin gene (SLC11A3). Br J Haematol 2002;119:539–46. [PubMed: 12406098]

16. Rivard SR, Lanzara C, Grimard D, Carella M, Simard H, Ficarella R, Simard R, D'Adamo AP, De Braekeleer M, Gasparini P. Autosomal dominant reticuloendothelial iron overload (HFE type 4) due to a new missense mutation in the FERROPORTIN 1 gene (SLC11A3) in a large French-Canadian family. Haematologica 2003;88:824–6. [PubMed: 12857562]

17. Hetet G, Devaux I, Soufir N, Grandchamp B, Beaumont C. Molecular analyses of patients with hyperferritinemia and normal serum iron values reveal both L ferritin IRE and 3 new ferroportin (slc11A3) mutations. Blood 2003;102:1904–10. [PubMed: 12730114]

18. Arden KE, Wallace DF, Dixon JL, Summerville L, Searle JW, Anderson GJ, Ramm GA, Powell LW, Subramaniam VN. A novel mutation in ferroportin1 is associated with haemochromatosis in a Solomon Islands patient. Gut 2003;52:1215–7. [PubMed: 12865285]

19. Wallace DF, Clark RM, Harley HA, Subramaniam VN. Autosomal dominant iron overload due to a novel mutation of ferroportin1 associated with parenchymal iron loading and cirrhosis. J Hepatol 2004;40:710–3. [PubMed: 15030991]

20. Jouanolle AM, Douabin-Gicquel V, Halimi C, Loreal O, Fergelot P, Delacour T, de Lajarte-Thirouard AS, Turlin B, Le Gall JY, Cadet E, Rochette J, David V, Brissot P. Novel mutation in ferroportin 1 gene is associated with autosomal dominant iron overload. J Hepatol 2003;39:286–9. [PubMed: 12873829]

21. Gordeuk VR, Caleffi A, Corradini E, Ferrara F, Jones RA, Castro O, Onyekwere O, Kittles R, Pignatti E, Montosi G, Garuti C, Gangaidzo IT, Gomo ZAR, Moyo VM, Rouault TA, MacPhail P, Pietrangelo A. Iron overload in Africans and African-Americans and a common mutation in the SCL40A1 (ferroportin 1) gene. Blood Cells Molecules and Diseases 2003;31:299–304.

22. Beutler E, Barton JC, Felitti VJ, Gelbart T, West C, Lee PL, Waalen J, Vulpe C. Ferroportin 1 (SCL40A1) variant associated with iron overload in African-Americans. Blood Cells Mol Dis 2003;31:305–9. [PubMed: 14636643]

23. Cremonesi L, Forni GL, Soriani N, Lamagna M, Fermo I, Daraio F, Galli A, Pietra D, Malcovati L, Ferrari M, Camaschella C, Cazzola M. Genetic and clinical heterogeneity of ferroportin disease. Br J Haematol 2005;131:663–70. [PubMed: 16351644]

24. Robson KJH, Merryweather-Clarke AT, Cadet E, Viprakasit V, Zaahl MG, Pointon JJ, Weatherall DJ, Rochette J. Recent advances in understanding haemochromatosis: a transition state. Journal of Medical Genetics 2004;41:721–730. [PubMed: 15466004]

25. Sham RL, Phatak PD, West C, Lee P, Andrews C, Beutler E. Autosomal dominant hereditary hemochromatosis associated with a novel ferroportin mutation and unique clinical features. Blood Cells Molecules and Diseases 2005;34:157–161.

26. Liu XB, Yang F, Haile DJ. Functional consequences of ferroportin 1 mutations. Blood Cells Mol Dis 2005;35:33–46. [PubMed: 15935710]

27. Schimanski LM, Drakesmith H, Merryweather-Clarke AT, Viprakasit V, Edwards JP, Sweetland E, Bastin JM, Cowley D, Chinthammitr Y, Robson KJ, Townsend AR. In vitro functional analysis of human ferroportin (FPN) and hemochromatosis-associated FPN mutations. Blood 2005;105:4096–102. [PubMed: 15692071]

28. Drakesmith H, Schimanski LM, Ormerod E, Merryweather-Clarke AT, Viprakasit V, Edwards JP, Sweetland E, Bastin JM, Cowley D, Chinthammitr Y, Robson KJH, Townsend ARM. Resistance to hepcidin is conferred by hemochromatosis-associated mutations of ferroportin. Blood 2005;106:1092–1097. [PubMed: 15831700]
29. De Domenico I, McVey Ward D, Nemeth E, Ganz T, Corradini E, Ferrara F, Musci G, Pietrangelo A, Kaplan J. Molecular and clinical correlates in iron overload associated with mutations in ferroportin. Haematologica 2006;91:1092–5. [PubMed: 16885049]
30. De Domenico I, Ward DM, Nemeth E, Vaughn MB, Musci G, Ganz T, Kaplan J. The molecular basis of ferroportin-linked hemochromatosis. Proc Natl Acad Sci U S A 2005;102:8955–60. [PubMed: 15956209]
31. Drakesmith H, Schimanski LM, Ormerod E, Merryweather-Clarke AT, Viprakasit V, Edwards JP, Sweetland E, Bastin JM, Cowley D, Chinthammitr Y, Robson KJ, Townsend AR. Resistance to hepcidin is conferred by hemochromatosis-associated mutations of ferroportin. Blood 2005;106:1092–7. [PubMed: 15831700]
32. Krautwurst D, Yau KW, Reed RR. Identification of ligands for olfactory receptors by functional expression of a receptor library. Cell 1998;95:917–26. [PubMed: 9875846]
33. Hu YK, Kaplan JH. Site-directed chemical labeling of extracellular loops in a membrane protein. The topology of the Na,K-ATPase alpha-subunit. J Biol Chem 2000;275:19185–91. [PubMed: 10764750]
34. Folta-Stogniew E. Oligomeric states of proteins determined by size-exclusion chromatography coupled with light scattering, absorbance, and refractive index detectors. Methods Mol Biol 2006;328:97–112. [PubMed: 16785643]
35. Wen J, Arakawa T, Philo JS. Size-exclusion chromatography with on-line light-scattering, absorbance, and refractive index detectors for studying proteins and their interactions. Anal Biochem 1996;240:155–66. [PubMed: 8811899]
36. Goncalves AS, Muzeau F, Blaybel R, Hetet G, Driss F, Delaby C, Canonne-Hergaux F, Beaumont C. Wild-type and mutant ferroportins do not form oligomers in transfected cells. Biochem J 2006;396:265–75. [PubMed: 16457665]
37. De Domenico I, Ward DM, Musci G, Kaplan J. Evidence for the multimeric structure of ferroportin. Blood 2007;109:2205–2209. [PubMed: 17077321]
38. Schimanski LM, Drakesmith H, Talbott C, Horne K, James JR, Davis SJ, Sweetland E, Bastin J, Cowley D, Townsend AR. Ferroportin: lack of evidence for multimers. Blood Cells Mol Dis 2008;40:360–9. [PubMed: 17977032]
39. Kawate T, Gouaux E. Fluorescence-detection size-exclusion chromatography for precrystallization screening of integral membrane proteins. Structure 2006;14:673–81. [PubMed: 16615909]
40. Nakano A. Spinning-disk confocal microscopy -- a cutting-edge tool for imaging of membrane traffic. Cell Struct Funct 2002;27:349–55. [PubMed: 12502889]
41. Pignatti E, Mascheroni L, Sabelli M, Barelli S, Biffo S, Pietrangelo A. Ferroportin is a monomer in vivo in mice. Blood Cells Molecules and Diseases 2006;36:26–32.
42. Sahin-Toth M, Lawrence MC, Kaback HR. Properties of permease dimer, a fusion protein containing two lactose permease molecules from Escherichia coli. Proc Natl Acad Sci U S A 1994;91:5421–5. [PubMed: 8202501]
43. Horiuchi M, Nicke A, Gomeza J, Aschrafi A, Schmalzing G, Betz H. Surface-localized glycine transporters 1 and 2 function as monomeric proteins in Xenopus oocytes. Proc Natl Acad Sci U S A 2001;98:1448–53. [PubMed: 11171971]
44. De Domenico I, Nemeth E, Nelson JM, Phillips JD, Ajioka RS, Kay MS, Kushner JP, Ganz T, Ward DM, Kaplan J. The hepcidin-binding site on ferroportin is evolutionarily conserved. Cell Metab 2008;8:146–56. [PubMed: 18680715]
45. Rivera S, Nemeth E, Gabayan V, Lopez MA, Farshidi D, Ganz T. Synthetic hepcidin causes rapid dose-dependent hypoferremia and is concentrated in ferroportin-containing organs. Blood 2005;106:2196–9. [PubMed: 15933050]
46. Krogh A, Larsson B, von Heijne G, Sonnhammer EL. Predicting transmembrane protein topology with a hidden Markov model: application to complete genomes. J Mol Biol 2001;305:567–80. [PubMed: 11152613]

47. Pietrangelo A, Montosi G, Totaro A, Garuti C, Conte D, Cassanelli S, Fraquelli M, Sardini C, Vasta F, Gasparini P. Hereditary hemochromatosis in adults without pathogenic mutations in the hemochromatosis gene. N Engl J Med 1999;341:725–32. [PubMed: 10471458]

48. Corradini E, Montosi G, Ferrara F, Caleffi A, Pignatti E, Barelli S, Garuti C, Pietrangelo A. Lack of enterocyte iron accumulation in the ferroportin disease. Blood Cells Molecules and Diseases 2005;35:315–318.

49. Roetto A, Merryweather-Clarke AT, Daraio F, Livesey K, Pointon JJ, Barbabietola G, Piga A, Mackie PH, Robson KJ, Camaschella C. A valine deletion of ferroportin 1: a common mutation in hemochromastosis type 4. Blood 2002;100:733–4. [PubMed: 12123233]

50. Njajou OT, de Jong G, Berghuis B, Vaessen N, Snijders P, Goossens JP, Wilson JHP, Breuning MH, Oostra BA, Heutink P, Sandkuijl LA, van Duijn CM. Dominant hemochromatosis due to N144H mutation of SLC11A3: Clinical and biological characteristics. Blood Cells Molecules and Diseases 2002;29:439–443.

51. Strop P, Brunger AT. Refractive index-based determination of detergent concentration and its application to the study of membrane proteins. Protein Science 2005;14:2207–2211. [PubMed: 16046633]

52. Gasteiger E, Gattiker A, Hoogland C, Ivanyi I, Appel RD, Bairoch A. ExPASy: The proteomics server for in-depth protein knowledge and analysis. Nucleic Acids Res 2003;31:3784–8. [PubMed: 12824418]

53. van der Merwe PA, Brown MH, Davis SJ, Barclay AN. Affinity and kinetic analysis of the interaction of the cell adhesion molecules rat CD2 and CD48. Embo J 1993;12:4945–54. [PubMed: 7903240]

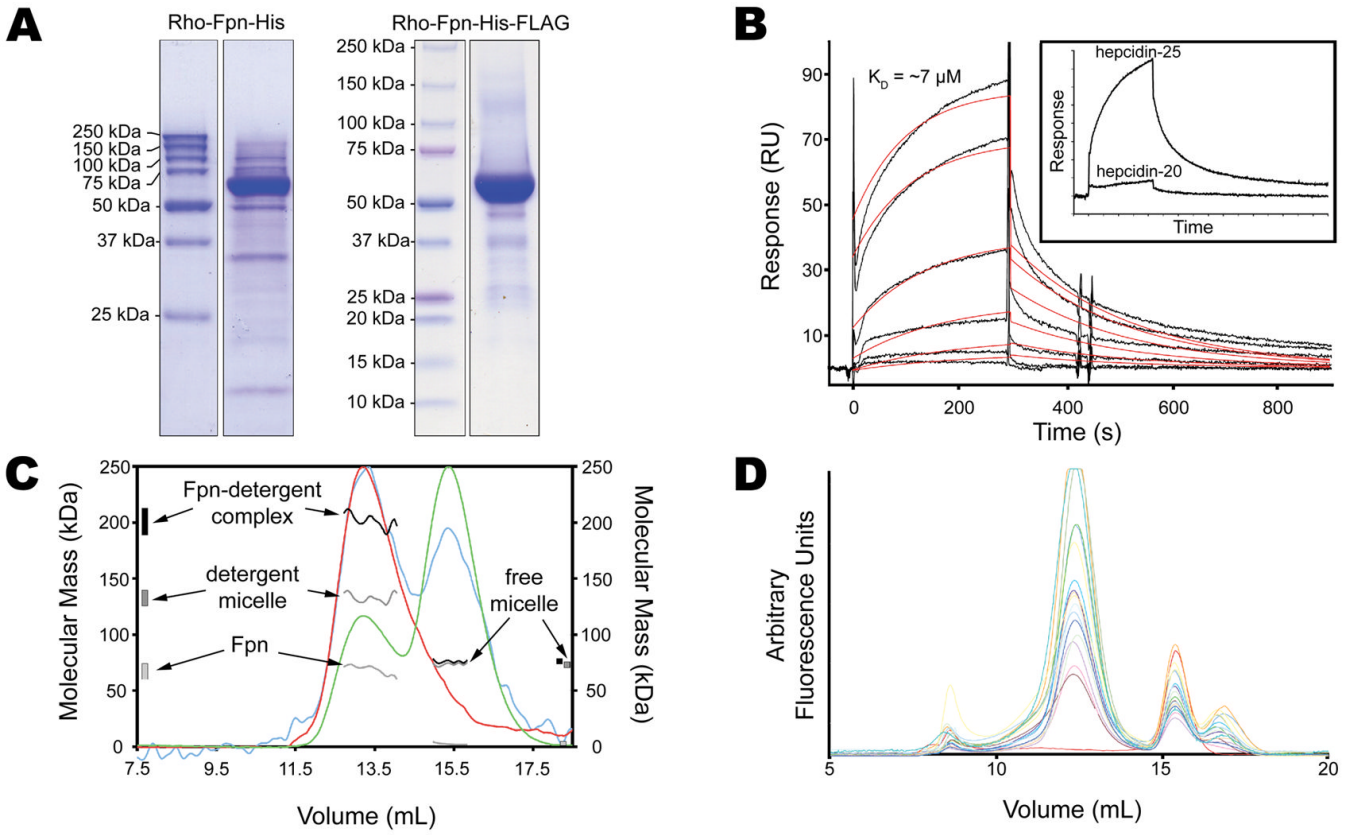

Figure 1. Biophysical Characterization of purified Fpn

(A) SDS-PAGE analysis of purified Rho-Fpn-His (estimated to be ~ 70% pure) and Rho-Fpn-His-FLAG (estimated to be ~ 90% pure) proteins. Samples were run under reducing conditions in SDS loading buffer without boiling on a 15% (Rho-Fpn-His) or 4–20% (Rho-Fpn-His-FLAG) polyacrylamide gel. (B) Biosensor analysis of the Fpn/hepcidin interaction. Hepcidin-25 was injected over immobilized Fpn as a series of dilutions (0.625, 1.25, 2.5, 5.0, 8.0, and 10 μM). Sensorgrams (black lines) are overlaid on the simulated response (red lines) derived using a 1:1 binding model. The fit of the binding model to the data is poor, perhaps resulting from the presence of hepcidin-25 aggregates. Inset shows results from injections of 10 μM hepcidin-25 and hepcidin-20. (C) SEC-LS/UV/RI analysis of DDM-solubilized Fpn. Normalized traces for UV absorbance at 280 nm (red), 90° LS signal (blue), and differential RI (green) signals are shown. Molecular mass values calculated for the protein-detergent complex (black), detergent micelle (dark grey), and protein (light grey) are displayed as overlays on the peaks at ~ 13.5 mL and ~ 15.5 mL, and the range of calculated molecular masses are projected onto the left and right axes. (D) Comparison of mobility by FSEC for wild-type Fpn versus disease-related Fpn mutants. Wild-type Fpn and 16 Fpn mutants were transiently expressed as GFP fusion proteins in HEK293T cells. Whole cell lysates were passed over a gel filtration column and the migration of each protein was monitored by fluorescence. Wild-type Fpn-GFP and all of the Fpn-GFP mutants exhibited a peak at ~ 12 mL, which was not found in lysates from untransfected HEK293T cells (red curve). The peak at ~ 16 mL was found in samples prepared from both transfected and untransfected cells.

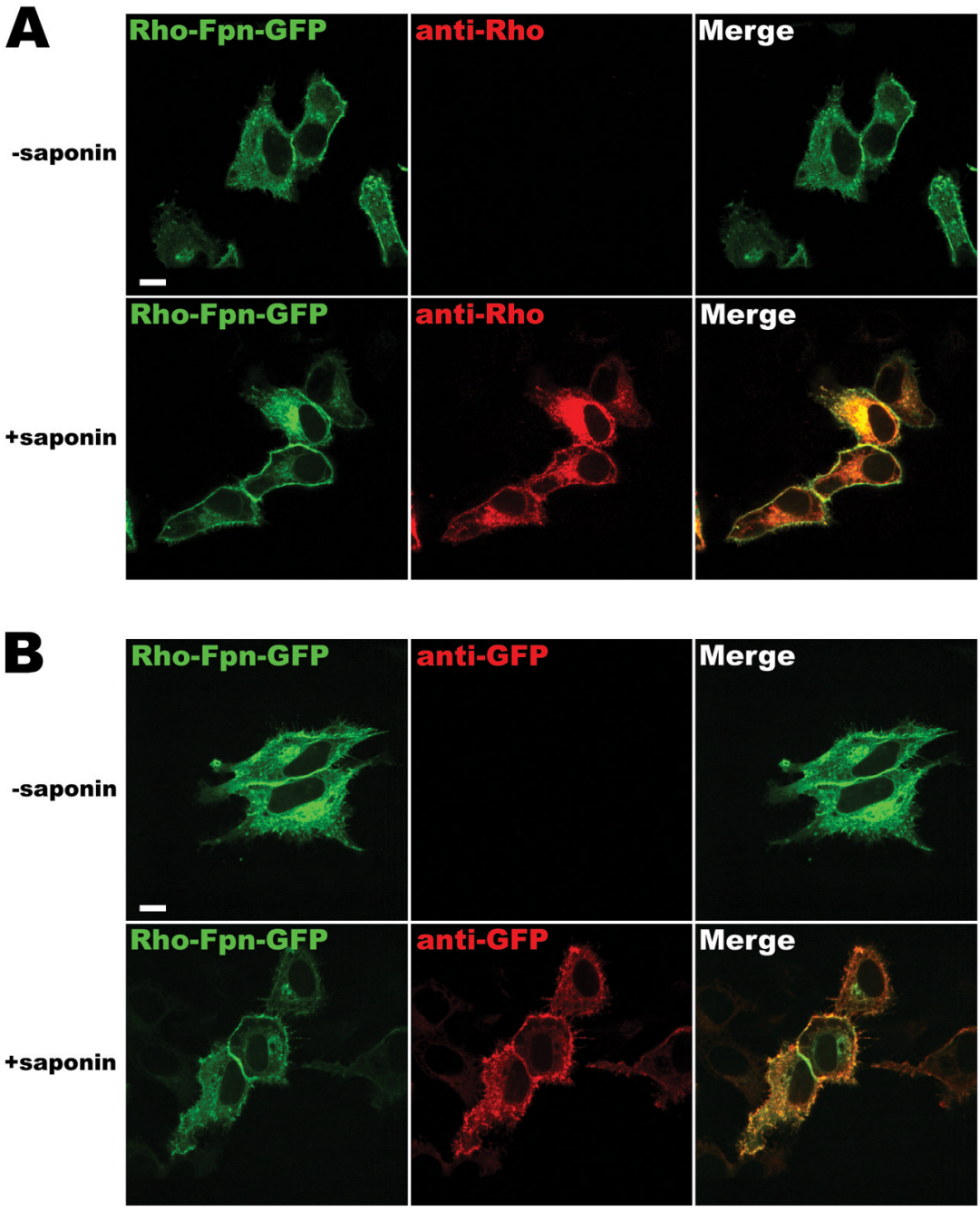

Figure 2. Analysis of Fpn membrane topology

Bar = 10 μm. Rho-Fpn-GFP was transiently expressed in HeLa cells. Fixed cells were probed against a labeled antibody against the N-terminal Rho tag (panel A) or against the C-terminal GFP tag (panel B) under permeabilizing (+ saponin) and non-permeabilizing (− saponin) conditions. Similar results were found for Rho-Fpn-GFP expressed in HEK293T and MDCK cells and for Fpn-GFP expressed in HeLa, HEK293T (Figure 9) and MDCK cells (data not shown).

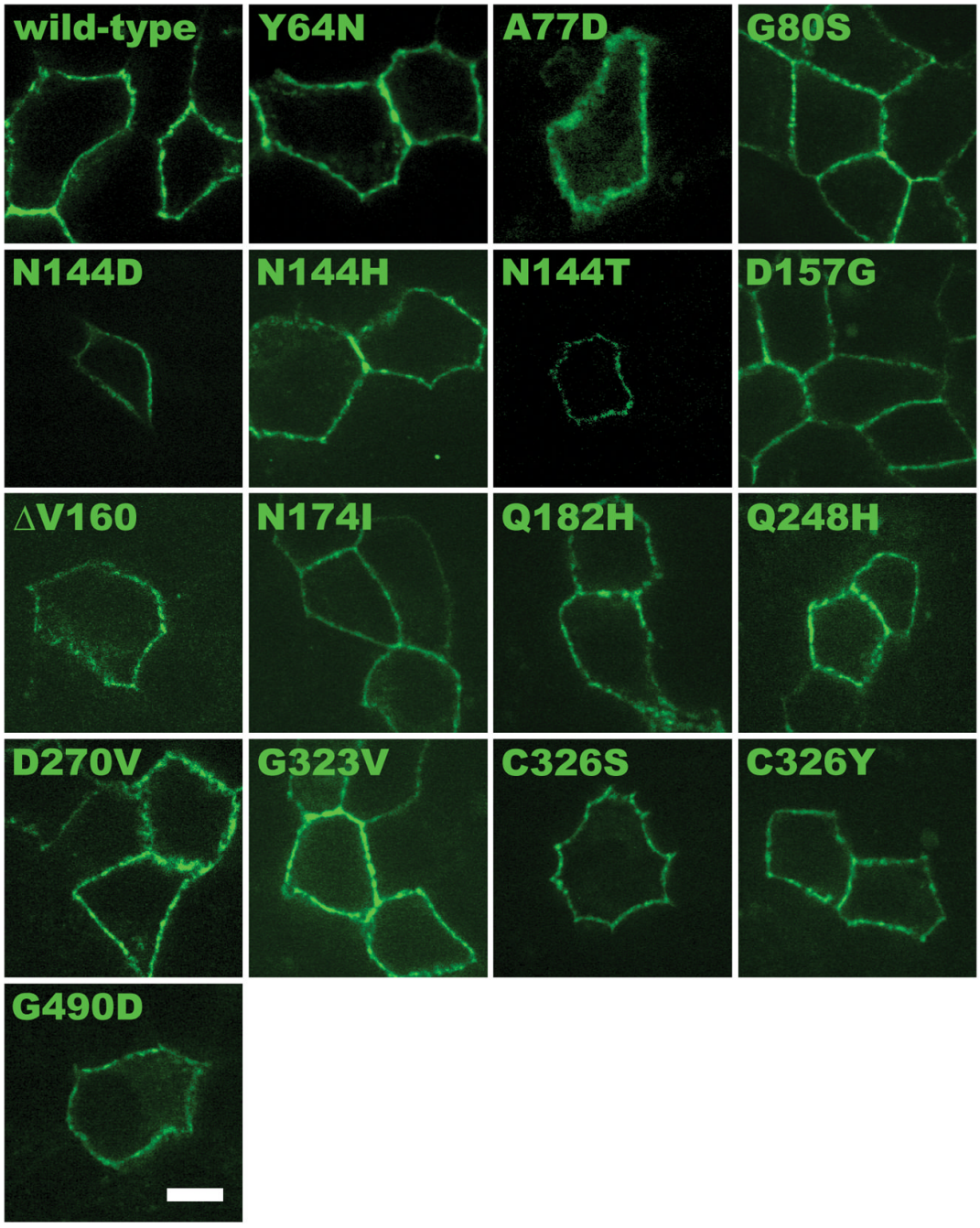

Figure 3. Fpn-GFP subcellular localization in MDCK cells

Bar = 10 μm. Fpn-GFP and disease-related Fpn-mutants were transiently expressed in filter-grown polarized MDCK cells.

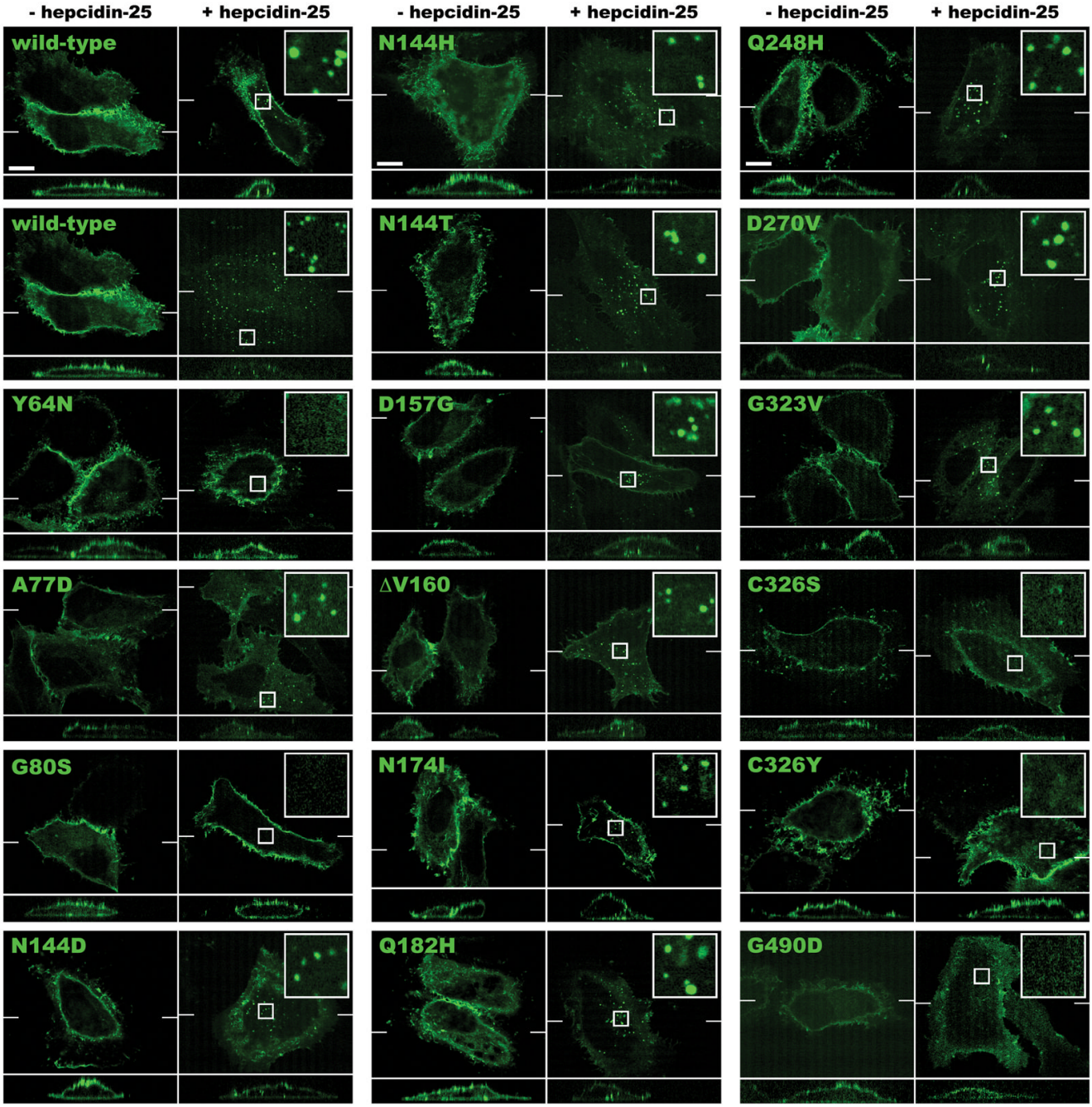

Figure 4. Fpn-GFP localization and sensitivity to hepcidin-25

Bar = 10 μm; inset is 5x original magnification. Fpn-GFP and disease-related Fpn-GFP mutants were transiently expressed in HeLa cells, which were pre-treated with cycloheximide and then incubated for 4 hours with or without 2 μM hepcidin-25. Each panel is a representative slice from a confocal stack. Below each panel is a reconstructed side view for the region in a plane denoted by the thin white line in the main panel. The side views were elongated by a factor of two in the z-direction to facilitate visualization of fluorescence in these thin cells.

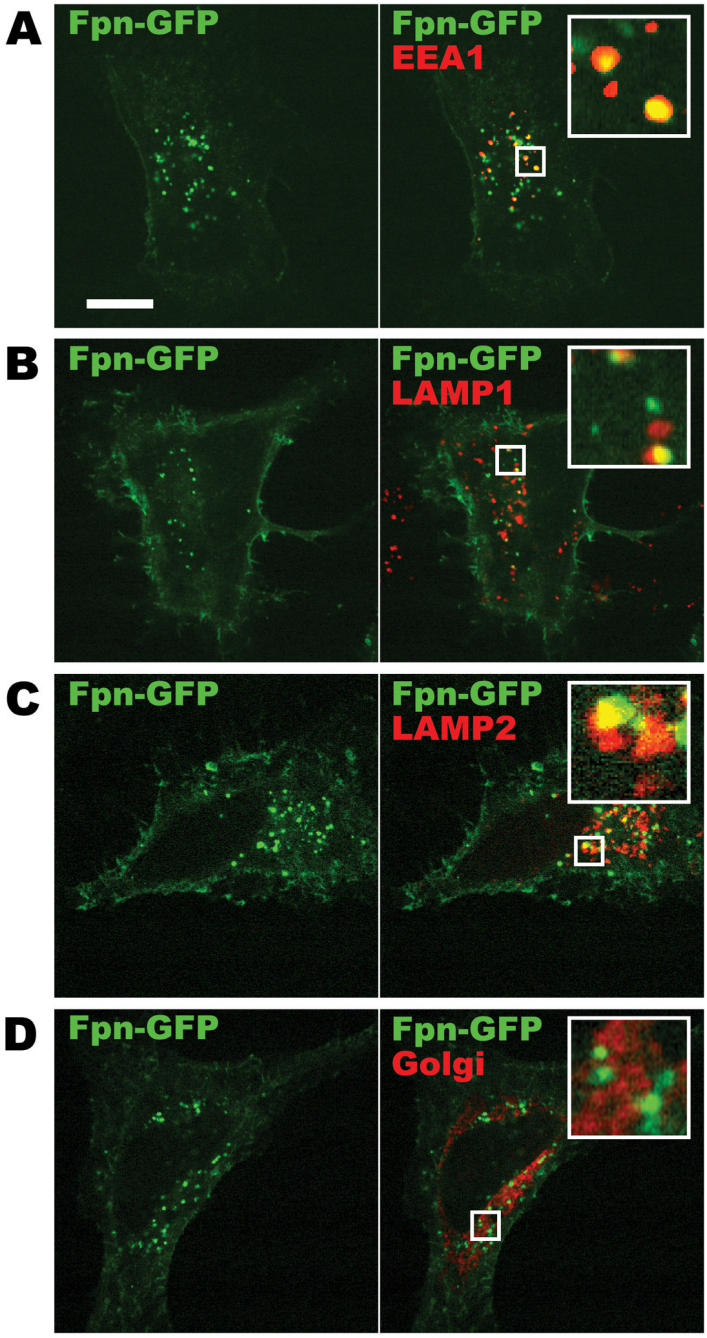

Figure 5. Mapping of the intracellular locations of hepcidin-internalized Fpn-GFP

Bar = 10 μm; inset is 5x original magnification. (A–D) Fpn-GFP was transiently expressed in HeLa cells, which were pre-treated with cycloheximide, incubated with 2 μM hepcidin-25. Fixed cells were probed with antibodies against markers for early endosomes (EEA1, panel A), lysosomes (LAMP1 and LAMP2, panels B and C), and the Golgi (58 kD Golgi protein, panel D). LAMP1 staining adjacent to the Fpn-GFP-positive cell in panel B represents endogenous LAMP1 from a neighboring cell that did not express Fpn-GFP.

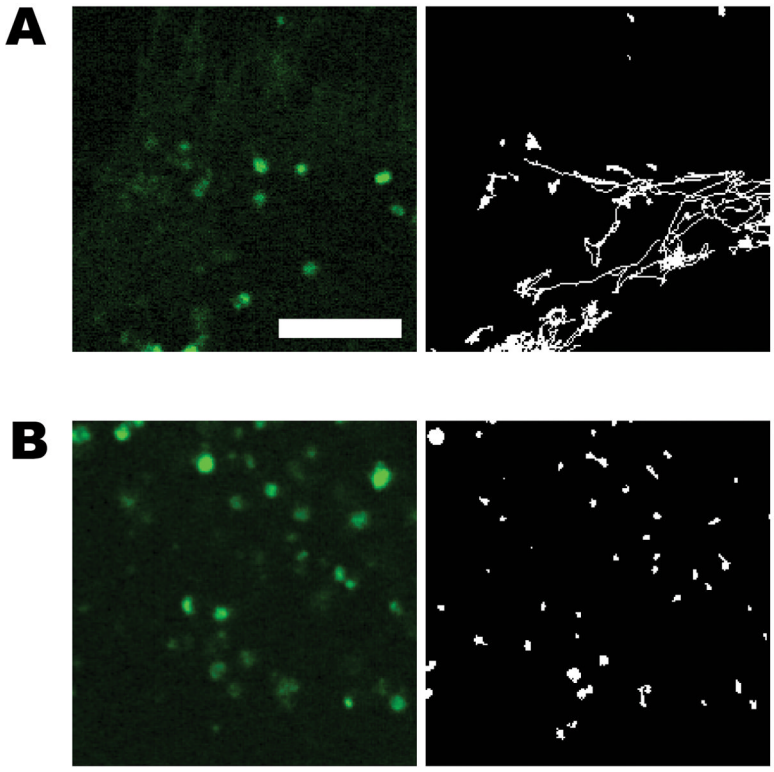

Figure 6. Effects of nocodazole on internalized Fpn

Bar = 5 μm. Fpn-GFP was transiently expressed in HeLa cells, which were pre-treated with cycloheximide, incubated with 2 μM hepcidin-25, and then imaged live in the presence or absence of 10 μg/mL nocodazole. GFP-positive compartments were tracked as described in the Methods. Tracks throughout a 90 second time course were overlaid on representative images of an untreated (panel A) or nocodazole-treated (panel B) cell.

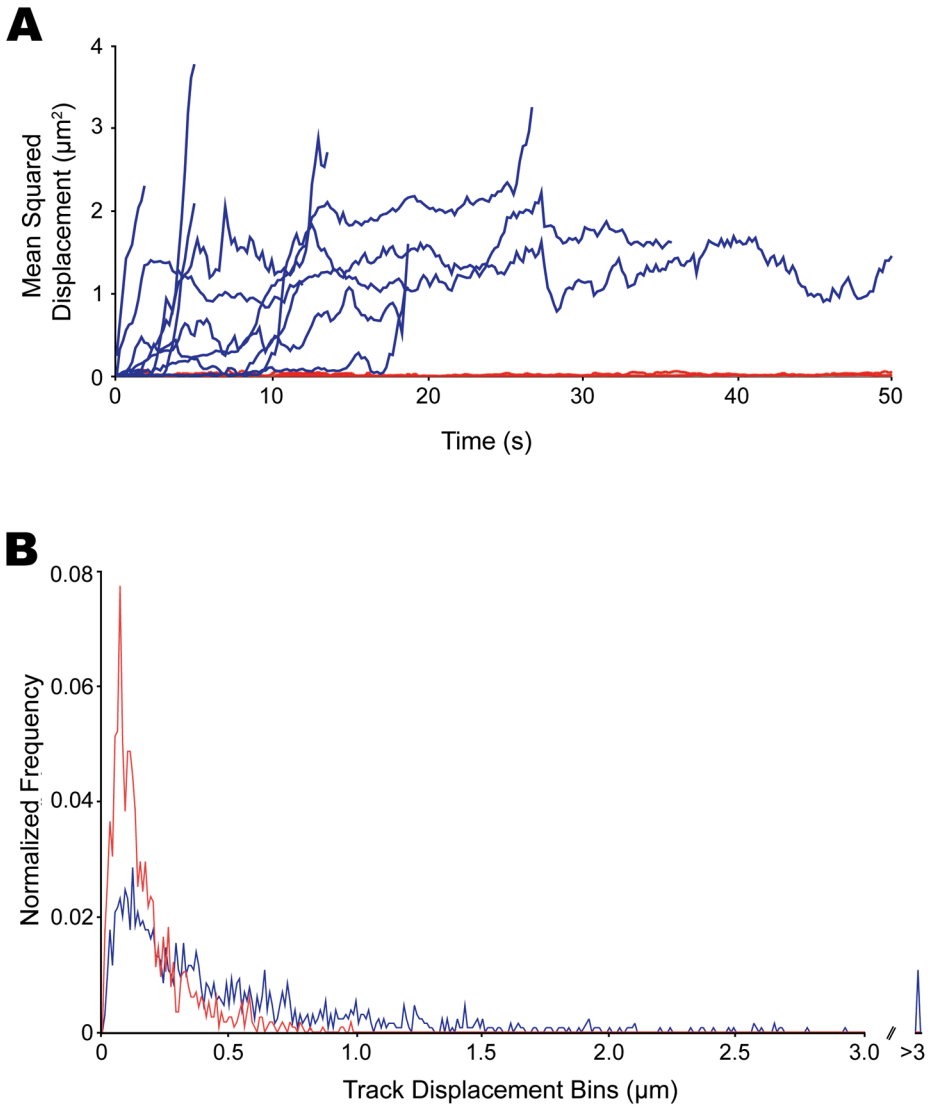

Figure 7. Tracking Fpn-GFP-positive compartments in HeLa cells in the presence and absence of nocodazole

Cells were treated and imaged as described in Figure 6. (A) The mean squared displacement of representative tracks in untreated (blue) versus nocodazole-treated (red) cells showed that nocodazole treatment produced a marked reduction in Fpn-GFP trafficking. (B) Track displacements for the set of tracked vesicles in untreated (blue) and nocodazole-treated (red) cells presented as a histogram.

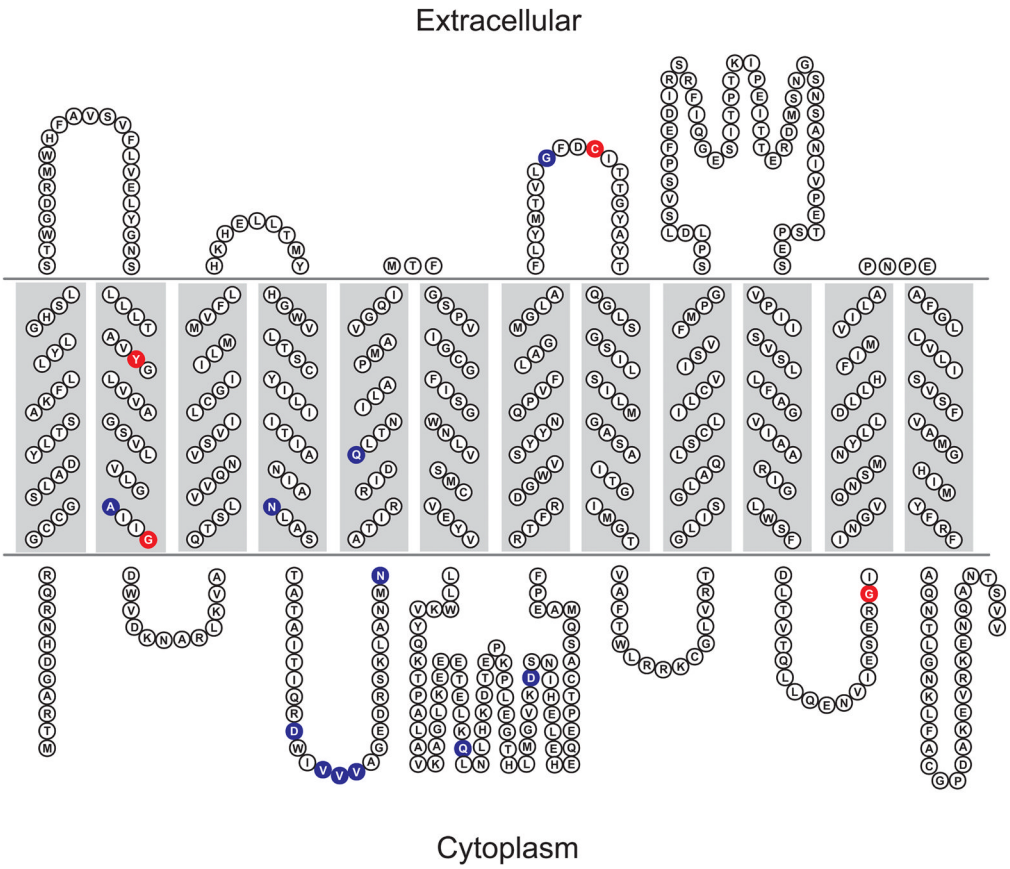

Figure 8. Prediction of membrane topology of Fpn

Sequences for full length human, mouse and zebrafish Fpns were submitted to the TMHMM v2.0 prediction server.[46] Each sequence was predicted to contain 12 regions that were 21–23 amino acids long with a significant (>60%) probability of being a transmembrane (TM) region (see Methods). TMHMM predicted that both the N- and C- termini of Fpn are cytosolic, consistent with our data (Figure 2 and 9). Highlighted amino acids indicate positions where disease-related mutations have been identified. Red positions indicate hepcidin-resistance and blue positions indicate hepcidin-sensitivity. Only the C326Y and C326S mutations fall in the hepcidin-binding domain, residues 324 to 343.[44]

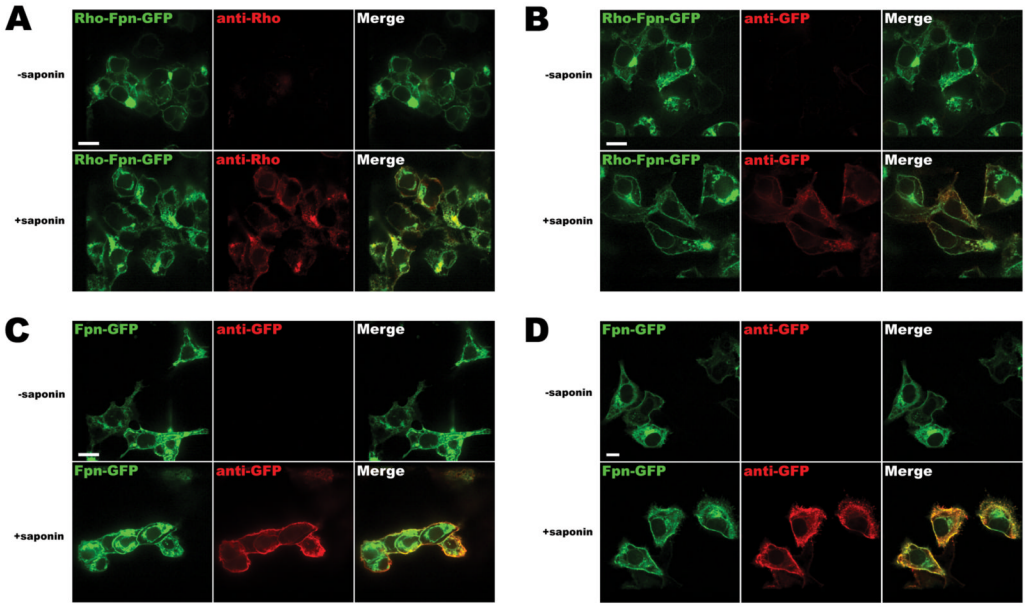

Figure 9. Analysis of Fpn membrane topology

Bar = 10 μm. (A-B) Rho-Fpn-GFP was transiently expressed in HEK293T cells. Fixed cells were probed against a labeled antibody against the N-terminal Rho tag (panel A) or against the C-terminal GFP tag (panel B) under permeabilizing (+ saponin) and non-permeabilizing (− saponin) conditions. (C–D) Fpn-GFP was transiently expressed in HEK293T (panel C) or HeLa (panel D) cells. Fixed cells were probed against a labeled antibody against the C-terminal GFP tag under permeabilizing (+ saponin) and non-permeabilizing (− saponin) conditions.